Indian Journal of Pure & Applied Physics
Vol. 42, September 2004, pp 653-665

Optoelectronic properties of mercuric iodide crystals for radiation detection

S L Sharma, G Anil Kumar & H N Acharya

Department of Physics & Meteorology, Indian Institute of Technology, Kharagpur 721 302

Received 12 December 2003; accepted 13 July 2004

Optoelectronic properties of some red mercuric iodide (α-HgI_2) crystals have been studied for wavelengths 450-700 nm at temperatures 80-300 K. These crystals were grown (a) by solvent evaporation from α-HgI_2-tetrahydrofurane saturated solution, (b) by hydration of α-HgI_2-dimethyl sulphoxide-methanol saturated solution and (c) by polymer controlled growth (PCG) in vapour phase. Important aspects of optical generation of the charge carriers have been discussed. The measurements of thermally stimulated currents were also carried out in order to understand the temperature dependence of photocurrents in different wavelength regions. With the computer simulation of the photocurrent versus wavelength spectrum, the room temperature transport properties (the mobility-lifetime products and surface recombination velocities of the two charge carriers) for the crystals of three types have been estimated. For a typical electric field strength of about 2×10^3 V/cm, the electron drift lengths for the crystals of three types were found to be 1150, 1350 and 6500 μm, respectively, whereas the hole drift lengths were found to be 50, 50 and 150 μm, respectively. As the typical thickness of α-HgI_2 photodetector for any scintillation spectrometer is about 300 μm, under the negative electrode illumination, all the three types of α-HgI_2 crystals present high potential for their use as photodetectors in conjunction with most of the scintillators.

[**Keywords**: Mercuric iodide; Photoresponse; Radiation detector; Scintillation spectrometer]

IPC Code: H 01 J 49/00

1 Introduction

Possessing large band gap (E_g = 2.13 eV at 300K) and high atomic number (80.53), since early 1970s, red mercuric iodide (α-HgI_2) has been considered to be one of the most promising semiconductor materials for room temperature operable X-ray and γ-ray detectors[1]. This led to an extensive study on the material processing, crystal growth and fabrication of detectors and X-ray and γ-ray detection properties of this material[2]. Recently, α-HgI_2 single crystals have also been used as photodetectors in scintillation spectrometers based on CsI(Tl), NaI(Tl), $CaWO_4$ and BGO scintillating materials[3-6]. In the α-HgI_2 photodetector based scintillation spectrometer, generation of the charge carriers in the α-HgI_2 crystal attached to the scintillating crystal solely depends upon the light emission of the scintillating crystal. Therefore, it is highly desired to study the photoresponse (i.e., photocurrent versus wavelength spectrum) of α-HgI_2 single crystals grown by different growth techniques in order to be able to understand the potential of α-HgI_2 photodetector based scintillation spectrometers. It may be noted that the region of highest photosensitivity of α-HgI_2 crystals coincides with the spectral region (i.e., wavelength range 400-700 nm) of maximum light emission of the above scintillating materials.

Till date, photocurrents for solution grown as well as for vapour phase grown α-HgI_2 single crystals were studied in order to determine the band gap energy, the temperature variation of the band gap energy[7], the carrier trapping levels[8], the lifetimes and surface recombination velocities of charge carriers[9-10]. Burshtein *et al.*[9] studied the photoresponse of TOM crystals (the crystals grown by temperature oscillation method) under the low and high field conditions. They explained their observations using Many's

model[11]. This model assumes that, in the long wavelength region, the whole of the crystal is uniformly illuminated. This means that, in the long wavelength region, the photogeneration is uniform throughout the bulk of the crystal. This approximation holds good only if the product of the absorption coefficient (α) and the crystal thickness (d) is very small as compared to unity. As will be pointed out later in this paper that the value of the absorption coefficient for a good quality α-HgI_2 single crystal in the long wavelength region ($\lambda > 600$ nm) is about 25-30 cm^{-1}, above approximation does not hold for crystals having thicknesses more than 50 μm. This may be the reason as to why the values of the electron and hole lifetimes reported by Burshtein *et al.*[9] greatly differ from the estimates of these parameters using X-ray excitations[12]. Bornstein and Bube[10] also studied the wavelength dependence of photoconductivity in TOM crystals in order to determine the diffusion lengths and lifetimes of electrons and holes. They analysed their measurements using De Vore's model[13] that is applicable only under zero-field conditions. For estimating the carrier lifetimes, however, they assumed constant values for the mobilities of electrons and holes.

As photoresponse determines the nuclear radiation detector grade of a photodetector for its use in any scintillation spectrometer, a detailed study was undertaken on the optoelectronic properties of α-HgI_2 crystals grown in our laboratory (a) by solvent evaporation from α-HgI_2-Tetrahydrofurane saturated solution, (b) by hydration of α-HgI_2-Dimethyl Sulphoxide-Methanol saturated solution and (c) by polymer controlled growth (PCG) in vapour phase. The study includes measurements on the wavelength dependence of photoconductivity at different temperatures in the temperature range 80-300 K and measurements on the thermally stimulated currents. The measurements on thermally simulated currents were made in order to understand the temperature dependence of the photoconductivity in terms of the ionization of filled-traps in the different wavelength regions.

Further, an algorithm has been developed for simulating the photoresponse. Using this algorithm, we simulated the room temperature photoresponse for each of the three types of crystals and obtained the optimized values of different transport properties such as the electron mobility-lifetime product ($\mu_e\tau_e$), hole mobility-lifetime product ($\mu_h\tau_h$), electron surface recombination velocity (S_e) and hole surface recombination velocity (S_h) for these crystals.

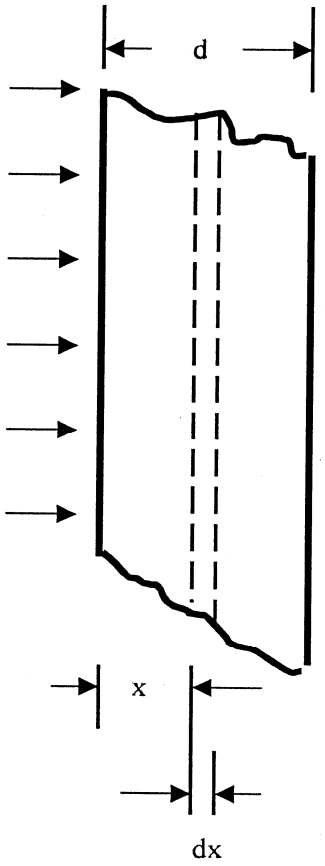

Fig. 1 — Typical thin parallel-faced photodetector under illumination

2 Theoretical Background

For a thin photodetector of thickness d (Fig. 1), whose one face is illuminated by normally incident optical radiation of intensity I_o (photons/cm^2.s), we have a weak absorption region ($h\nu < E_g$) and a strong absorption region ($h\nu \geq E_g$). For the weak absorption region, the photons have long penetration depths inside the photodetector. If the thickness of the photodetector is such that the product αd (α being the absorption coefficient) is much greater than unity for all wavelengths under study, then the effect of multiple reflections from the two (parallel) faces can be neglected. As has already been pointed out earlier

this is the case for α-HgI_2 photodetectors of thickness larger than 50 μm. Therefore, the intensity of the optical radiation $I(x)$ at a distance x from the illuminated face can be expressed as

$$I(x) = I_O \mathrm{e}^{-\alpha x} \quad \ldots(1)$$

The corresponding rate of generation of electron-hole pairs per unit volume around a point at a distance x from the illuminated surface can be written as

$$G = \beta\,\alpha\, I(x) = \beta\,\alpha\, I_O \mathrm{e}^{-\alpha x} \quad \ldots(2)$$

where, β denotes the photon quantum efficiency for electron-hole pair generation.

For the parallel plate electrode geometry, at high electric fields within the photodetector, the diffusion current can be neglected as compared to the drift current. Therefore, the net carrier density $n(x)$ at a distance x from the illuminated electrode can be expressed as

$$\frac{\mathrm{d}n}{\mathrm{d}t} = G - \frac{n}{\tau} \quad \ldots(3)$$

where, τ denotes the effective lifetime of the charge carriers. The solution of the above equation is

$$n(x) = G\,\tau\,[1 - \mathrm{e}^{-t/\tau}] = \beta\alpha I_o \tau\, \mathrm{e}^{-\alpha x}\,[1 - \mathrm{e}^{-t/\tau}] \quad \ldots(4)$$

Now, under the negative electrode illumination, the electron and hole current densities can, respectively, be written as

$$J_e^{(-)} = \left(\frac{1}{d}\right) \int_0^d q\,\mu_e E\, n(x)\,\mathrm{d}x$$

$$= \left(\frac{q\, d_e\, \beta\,\alpha\, I_O}{d}\right) \int_0^d \mathrm{e}^{-\alpha x} \left[1 - \mathrm{e}^{-\frac{d-x}{d_e}}\right] \mathrm{d}x$$

$$= \left(\frac{q\, d_e\, \beta\,\alpha\, I_O}{d}\right) \left[\left\{\frac{1 - \mathrm{e}^{-\alpha d}}{\alpha}\right\} + \left\{\frac{\mathrm{e}^{-\frac{d}{d_e}}\left(\mathrm{e}^{-d\left(\alpha - \frac{1}{d_e}\right)} - 1\right)}{\left(\alpha - \frac{1}{d_e}\right)}\right\}\right] \quad \ldots(5)$$

$$J_h^{(-)} = \left(\frac{q\, d_h\, \beta\,\alpha\, I_O}{d}\right) \left[\left\{\frac{1 - \mathrm{e}^{-\alpha d}}{\alpha}\right\} + \left\{\frac{\left(\mathrm{e}^{-d\left(\alpha + \frac{1}{d_h}\right)} - 1\right)}{\left(\alpha + \frac{1}{d_h}\right)}\right\}\right] \quad \ldots(6)$$

where, q is the electronic charge, E the electric field inside the photodetector, d_e (= $\mu_e\tau_e E$) the electron drift length, d_h (= $\mu_h\tau_h E$) the hole drift length, μ_e the electron mobility, μ_h the hole mobility, τ_e the electron lifetime and τ_h the hole lifetime .

Thus, under the negative electrode illumination, the total current density is given by

$$J^{(-)} = J_e{}^{(-)} + J_h{}^{(-)}$$

$$= \left(\frac{q\beta\alpha I_O}{d}\right)\left[\left(d_e + d_h\right)\left\{\frac{1-\mathrm{e}^{-\alpha d}}{\alpha}\right\} + d_e\left\{\mathrm{e}^{-\frac{d}{d_e}}\frac{\left(\mathrm{e}^{-d\left(\alpha-\frac{1}{d_h}\right)}-1\right)}{\left(\alpha-\frac{1}{d_e}\right)}\right\} + d_h\left\{\frac{\mathrm{e}^{-d\left(\alpha+\frac{1}{d_h}\right)}-1}{\alpha+\frac{1}{d_h}}\right\}\right] \quad \ldots(7)$$

Similarly, under the positive electrode illumination, the total current density is given by

$$J^{(+)} = J_e{}^{(+)} + J_h{}^{(+)}$$

$$= \frac{\left(q\beta\alpha I_O\right)}{d}\left[\left(d_e + d_h\right)\left\{\frac{1-\mathrm{e}^{-\alpha d}}{\alpha}\right\} + d_e\left\{\frac{\left(\mathrm{e}^{-d\left(\alpha+\frac{1}{d_e}\right)}-1\right)}{\alpha+\frac{1}{d_e}}\right\} + d_h\left\{\left(\mathrm{e}^{-\frac{d}{d_h}}\right)\frac{\left(\mathrm{e}^{-d\left(\alpha-\frac{1}{d_h}\right)}-1\right)}{\left(\alpha-\frac{1}{d_h}\right)}\right\}\right] \quad \ldots(8)$$

For the photons of energy $h\nu \geq E_g$, the light is absorbed within a very thin layer of the photodetector as compared to its thickness d. The generation of electron-hole pairs can, therefore, be assumed to be zero everywhere in the bulk of the photodetector except at the illuminated surface, where the generation rate per unit area is given by $G_s = \beta I_o$. So, under the negative electrode illumination only electrons and under the positive electrode illumination only holes are injected into the bulk of the medium. Therefore, under the negative electrode illumination, we can write

$$G_S = [\mu_e E + S_e] n_e(\mathrm{o}) \quad \ldots(9)$$

where, $n_e(\mathrm{o})$ is the surface electron density and S_e denotes the rate of surface recombination for each electron (i.e., the electron surface recombination velocity). The first term on the right side of the above equation represents the particle current leaving the surface and the second term represents the rate of surface recombination. From Eq. (9), we get

$$n_e(\mathrm{o}) = \frac{\beta I_O}{\mu_e E + S_e} \quad \ldots(10)$$

So, the electron density at any point at a distance x from the illuminated surface can be written

$$n_e(x) = \left(\frac{\beta I_O}{\mu_e E + S_e} \right) e^{-\frac{x}{d_e}} \quad \ldots(11)$$

Thus, under the negative electrode illumination, the photocurrent density becomes

$$J_S^{(-)} = \left\{ \frac{q \beta I_O}{[\mu_e E + S_e]} \right\} \left\{ \frac{\mu_e E}{d} \right\} \int_o^d e^{-x/d_e} \, dx$$

$$= \left\{ \frac{q \beta I_O}{\left[1 + \frac{S_e}{\mu_e E} \right]} \right\} \left\{ \frac{d_e}{d} \right\} \left[1 - e^{-d/d_e} \right] \quad \ldots(12)$$

Similarly, under the positive electrode illumination, the photocurrent density can be written as

$$J_S^{(+)} = \left\{ \frac{q \beta I_O}{\left[1 + \frac{S_h}{\mu_h E} \right]} \right\} \left\{ \frac{d_h}{d} \right\} \left[1 - e^{-d/d_h} \right] \quad \ldots(13)$$

where, S_h denotes the rate of surface recombination for each hole (i.e., the hole surface recombination velocity).

3 Experimental Details

Commercially available α-HgI_2 powder (E-MERCK: 98% assay) was purified by eight-time sublimation[2]. Crystals were then grown using the purified material (a) by solvent evaporation from α-HgI_2–Tetrahydrofurane saturated solution[14], (b) by hydration of α-HgI_2-Dimethyl Sulphoxide-Methanol saturated solution[15] and (c) by polymer controlled growth (PCG) technique in vapour phase[16].

Samples of sizes 5×5×1 mm^3 were cleaved perpendicular to the c-axis from large solution grown crystals and were etched in 10% aqueous KI solution for about 10 min. Platelet-shaped crystals grown by PCG technique were also etched in 10% aqueous KI solution for about 10 min. Electrical contacts were then made by painting thin layer of aquadag on the opposite faces of each of the samples. The samples were then fixed onto a circular copper plate for subsequent measurements.

For recording a photoconductivity spectrum, each time, a sample was mounted inside a cryostat. An electric field of about 2×10^3 V/cm was applied parallel to the c-axis of the sample. After cooling the sample to a desired temperature, the steady state photocurrents were recorded at different wavelengths in the wavelength range 450-700 nm for the three types of samples. The interval of wavelengths was chosen to be about 10 nm. The photoconductivity spectra were thus recorded at different temperatures in the temperature range 80-300 K for several etched samples of each of the three types under negative as well as positive electrode illumination. The beam of monochromatic light was obtained from an ORIEL lamp-monochromator assembly (Model Nos. 7340 and 77250, respectively). Photocurrents were measured with a KEITHLEY 610C electrometer amplifier. The photoconductivity spectra were subsequently analysed using the method outlined in the Sec.-2 for plate-shaped photodetectors.

For the measurements on the thermally stimulated currents (TSC), the sample under investigation was excited at liquid nitrogen temperature by means of photons of energy equal to the band gap energy at liquid nitrogen temperature. After filling the traps, the excitation was stopped and the sample was then heated in dark to 300 K at a constant heating rate of about 0.2 K/s. Measuring emf of a copper-constantan thermocouple placed close to the sample monitored the temperature of the sample. Accuracy of the temperature measurements was about ±1 K. The current in excess to the dark current, resulting due to the release of the trapped charge carriers into the valence band (for holes) or conduction band (for electrons), was monitored by a KEITHLEY 610C electrometer amplifier as a function of the temperature of the sample and was recorded on a X-Y recorder. In this manner, TSC spectra were recorded for several samples of each of the three types of crystals. Different peaks in a TSC spectrum represent different trapping levels. The TSC spectra were subsequently analysed using the method of Pal *et al.*[17]

4 Results and Discussion

The dark conductivity of the crystals of three types, at 300 K, was found to be of the order 10^{-13} Ω^{-1} cm^{-1}. From the room temperature (~ 300 K) optical absorption spectra for the three types of α-HgI_2 single crystals (Fig. 2) recorded using SHIMADZU UV-VIS spectrophotometer, the absorption coefficients were determined for the wavelengths 450-700 nm. The lowest value of the absorption coefficient (α) for solution grown crystals was found to be about 30 cm^{-1} and that for PCG crystals was found to be about 25 cm^{-1} in the wavelength region 600-700 nm. Also, from the absorption edges, the estimates of the band gap energy (E_g) for solution grown crystals was found to be about 2.13 eV and that for PCG crystals was found to be about 2.15 eV. These values match reasonably well with the values reported recently by Burger and Nason[18].

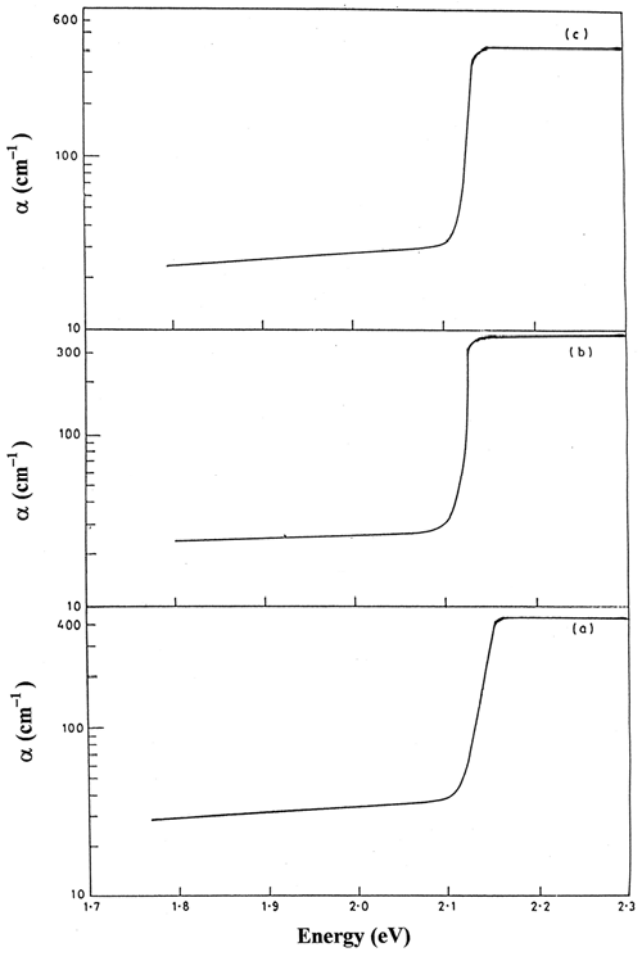

Fig. 2 — Typical absorption spectra for α-HgI_2 crystals of three types

The TSC measurements were performed on several samples made out of the three types of crystals. All the TSC spectra consisted of a number of peaks and some of them were not well resolved. The unresolved peaks were separated numerically. Although the peak heights varied from sample to sample, the temperatures corresponding to the peaks were not observed to change appreciably. The spectra and the results derived from them are more or less typical to each type of crystal and describe a general behaviour.

Fig. 3 shows the TSC spectra for three good quality THF crystals (the crystals grown by solvent evaporation from α-HgI_2-Tetrahydrofurane saturated solution). It is seen that these crystals, in general, possess four peaks at 135 K, 170 K, 195 K, 210 K and an intense peak at 275 K. The peaks at 135 K, 170 K, 195 K and 275 K are well resolved. Fig. 4 shows the TSC spectra for three α-HgI_2 crystals of good quality grown from DMSO-MeOH-α-HgI_2 saturated solution

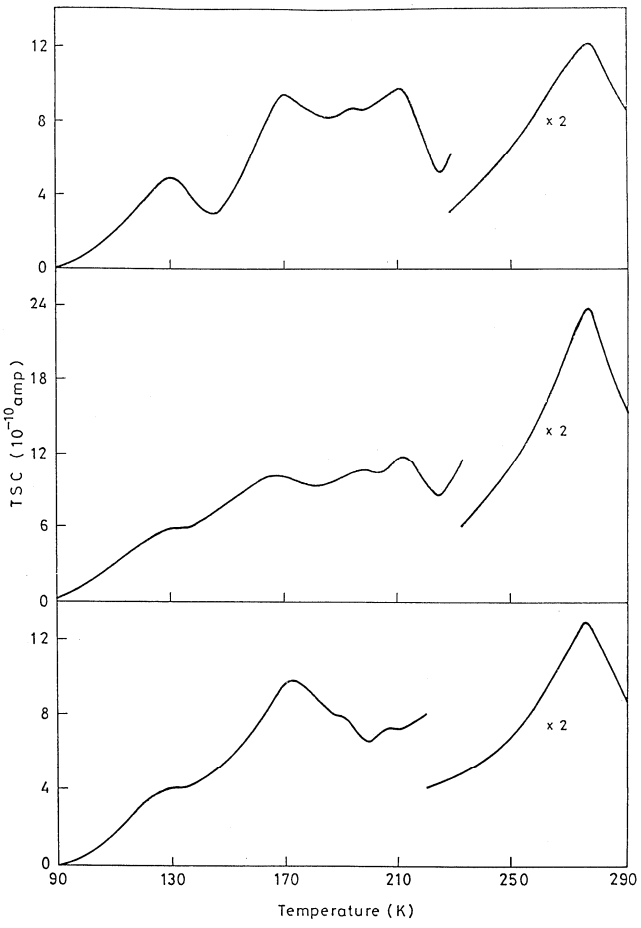

Fig. 3 — TSC spectra for three good quality THF crystals

(henceforth these crystals will be referred to as DMSO crystals). Each spectrum, in general, consists of five peaks at temperatures 135 K, 154 K, 173 K, 210 K and 235 K. The peaks at 135 K, 173 K and 235 K are well resolved. Fig. 5 shows the TSC spectra for three PCG crystals (the crystals grown by PCG technique in vapour phase). These spectra show only two well-resolved peaks corresponding to temperatures 170 K and 235 K and one weak peak at about 135 K.

The TSC peak temperatures, observed in the present study for the three types of crystals, match reasonably well with those reported in the literature[19]. In fact, present TSC peaks form a subset of the total of eleven TSC peaks reported so far[19]. The intense TSC peak at about 170-173K is common to all the three types of crystals used in the present study and is quite consistent with the previous reports[7,8,20-22]. According to Mohammed-Brahim *et al.*[8], De Blasi *et al.*[20] and Tadjine *et al.*[21], the detector grade α-HgI_2 crystals should possess a strong TSC peak at about 170K. Suryanarayana *et al.*[22] also observed a TSC peak at about 235 K in the case of DMSO crystals. They showed that the appearance of this peak was due to the iodine deficiency in the DMSO crystals grown by them. The crystals grown in the present study are expected to be non-stoichiometric. So, the peak at 235K, observed in the present study should be due to the lack of iodine in the grown crystals. However, quite surprisingly this peak was not observed in the TSC spectra of THF crystals. Possibly, the intense peak at about 275K that was not observed in the DMSO and PCG crystals overshadowed the peak at about 235K in the case of THF crystals. As reported by Bohac[14], the THF crystals may possess some inclusion of molecules of the mother liquor. Thus, this particular peak may be attributed to the inclusion of solvent molecules acting as organic impurities that may give rise to a deep trapping level. The origin of the other peaks is not yet understood. However, considering the number of TSC peaks in the three types of crystals, one may conclude that PCG crystals are of much better quality as compared to the solution grown crystals. Table 1 lists the activation energies of different TSC peaks, observed in the three types of crystals.

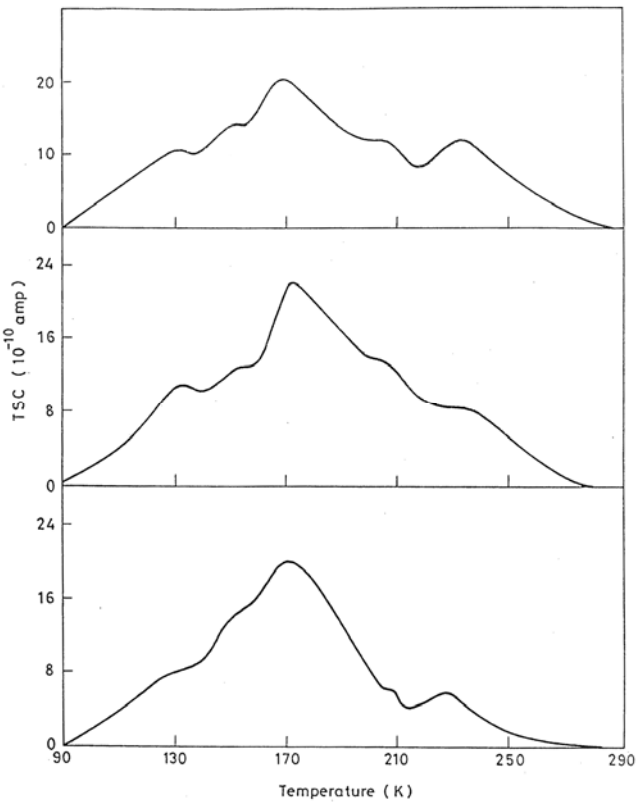

Fig. 4 — TSC spectra for three good quality DMSO crystals

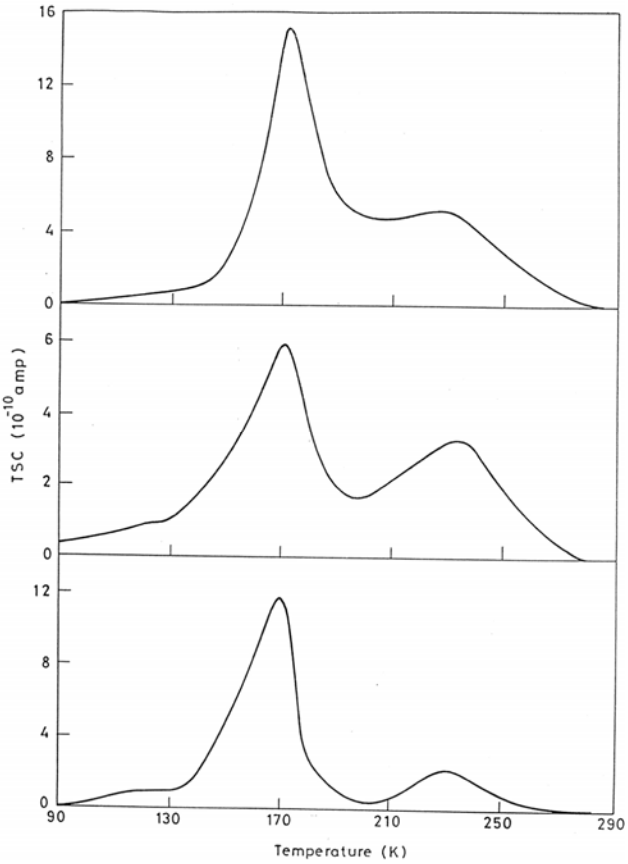

Fig. 5 — TSC spectra for three good quality PCG crystals

Table 1 — Temperatures of different TSC peaks along with activation energies of different trapping levels present in α-HgI_2 crystals of three types

Crystal type	TSC peak temperature T_m (K)	Activation energy (eV)
THF crystal	135	0.15
	170	0.31
	195	0.44
	210	0.50
	275	0.70
DMSO crystal	135	0.15
	154	0.22
	173	0.32
	210	0.44
	235	0.59
PCG crystal	135	0.15
	170	0.31
	235	0.59

Fig. 6 shows the typical photoconductivity spectra for the THF crystals at different temperatures under negative as well as positive electrode illumination. Similar spectra for the DMSO crystals and PCG crystals are shown in Figs 7 and 8, respectively. Each of these spectra was obtained by normalizing various regions of a recorded photoconductivity spectrum with respect to the photon flux of 5×10^{14} photons/cm^2.s at λ = 580 nm. The photoconductivity under negative electrode illumination is always higher than that under positive electrode illumination. This is quite similar to the observation of Bornstein and Bube[10] but is in contradiction with what Burshtein *et al.*[9] has reported. Surprisingly enough, both these groups performed their measurements on the crystals grown by temperature oscillation method. The higher values of the photoconductivity under negative electrode illumination as compared to those under positive electrode illumination, observed in the present study for all the three types of crystals, clearly indicate that the drift length for electrons is always much higher than that for holes.

The shapes of these photoconductivity spectra can be understood better if we divide each of these spectra into three spectral regions:

(i) The weak absorption region, where photoconductivity increases rapidly on lowering the wavelength, lies in the wavelength range 700-590 nm.

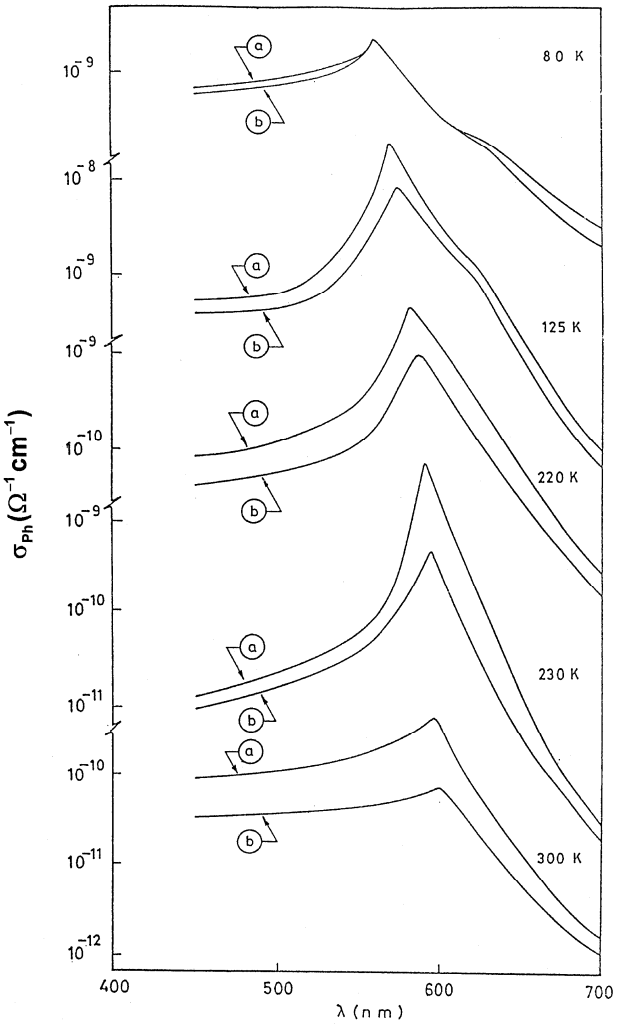

Fig. 6 — Typical photoconductivity spectra for THF crystals at different temperatures: (a) under the negative electrode illumination and (b) under the positive electrode illumination

In this spectral region, the absorption coefficient (α) for the three types of crystals is almost constant and is found to be about 28 ± 3 cm^{-1}.

(ii) The peak region lies in the wavelength range 590-550 nm. In this spectral region, each of the photoconductivity spectra possesses a sharp peak. The absorption coefficient (α) for the three types of crystals increase from about 28 ± 3 cm^{-1} to about 200 ± 20 cm^{-1}.

(iii) The strong absorption region, where photoconductivity decreases rather slowly on lowering the wavelength of the incident light, lies in the wavelength region below 550 nm. The absorption coefficient (α) for the three types of crystals is found to be about 410 ± 20 cm^{-1}.

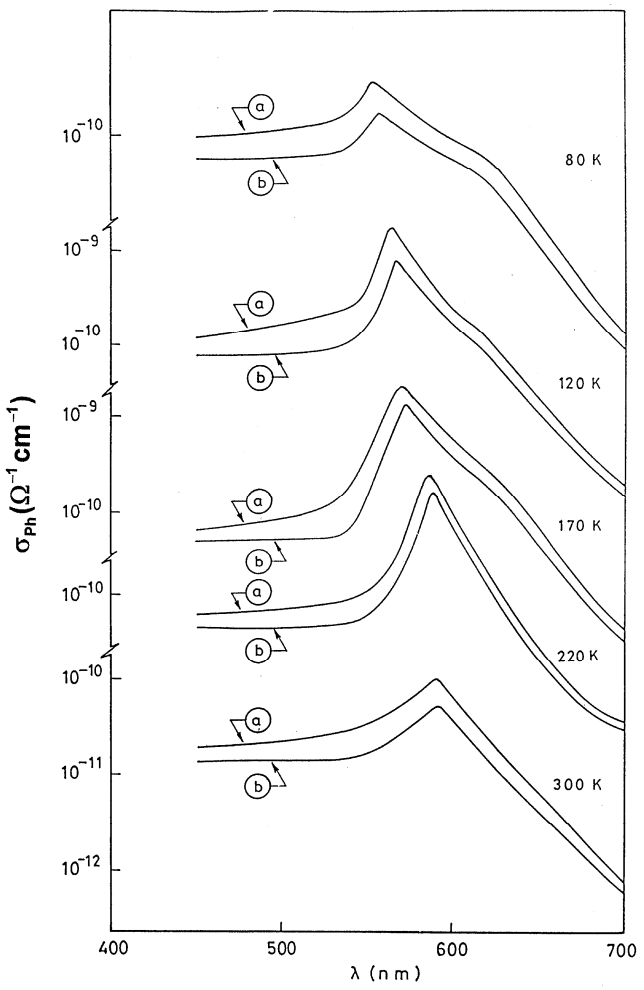

Fig. 7 — Typical photoconductivity spectra for DMSO crystals at different temperatures: (a) under the negative electrode illumination and (b) under the positive electrode illumination

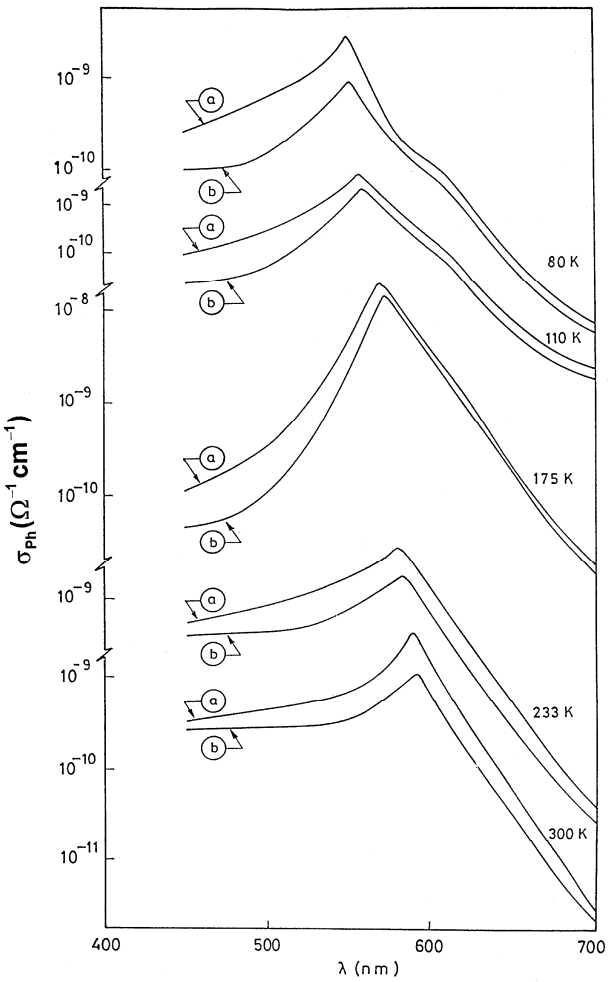

Fig. 8 — Typical photoconductivity spectra for PCG crystals at different temperatures: (a) under the negative electrode illumination and (b) under the positive electrode illumination

In the weak absorption region (700 nm ≥ wavelength ≥ 590 nm), for each of the three types of crystals separately, the photoconductivity spectra under negative and positive electrode illumination are expected to be identical if the charge carrier generation is assumed to be uniform throughout the bulk of the sample. Experimentally, however, the photoconductivity under negative electrode illumination is always higher. This clearly indicates that the charge carrier generation is not uniform. As the product αd is greater than unity for typical electrode separations of about 400 μm for all the three types of crystals, the carrier generation is more near the illuminated electrode and decreases quite appreciably along the thickness of the sample. Though the total photocurrent comprises of the contribution from the bulk as well as that from the surface, a direct calculation using Eqs (6), (7), (12) and (13) for the present case shows that the surface contribution in this region is negligible as compared to the bulk contribution (i.e. $J_s^{(-)}/J^{(-)}$ and $J_s^{(+)}/J^{(+)} \sim 10^{-3}$). This shows that the increase in the photoconductivity under negative electrode illumination at all wavelengths is due to an increase in the overall charge collection efficiency.

Further, in the weak absorption region, it is expected that a photoconductivity spectrum will be similar to the corresponding absorption spectrum. However, for each of the three types of crystals, the former shows a sharp rise that may be attributed to the large increase in the quantum efficiency (β) with the increase of energy of the incident light. The photoconductivity spectra recorded at low temperatures, for each of the three types of crystals,

show a shoulder at about 6200 Å. This observation is quite similar to that observed by Bube[7], Hyder[23] and Burshtein *et al.* [9]. Bube[7] and Hyder[23] also observed a photoluminescence peak at around 6200 Å in their crystals. Merz *et al.*[24] reported the disappearance of the photoluminescence peak at about 6200 Å upon purification. Recent studies on photoluminescence of α-HgI_2 single crystals by James *et al.*[25], however, confirmed the appearance of the band at around 6200Å in all the detector grade crystals with different relative intensities and slightly different energies. This band, previously thought to be due to impurities, showed no change in several doping experiments. The shoulder at about 6200 Å, observed in the low temperature photoconductivity spectra, has been confirmed by Lopez-Cruz[26] to be due to the indirect band gap in α-HgI_2 crystals at about 2.00 eV. The non-appearance of this shoulder in the photoconductivity spectra, recorded at higher temperatures for each of the three types of crystals, may be attributed to the shift of peaks in the photoconductivity spectra towards longer wavelength side at higher temperatures.

Around the peak region of the photoconductivity spectra, for each of the three types of crystals, the absorption coefficient (α) rises very rapidly from about 28±3 cm^{-1} to about 200 cm^{-1} as well as the quantum efficiency attains its maximum value. Therefore, the charge carrier concentration generated close to the illuminated electrode is expected to be many orders of magnitude higher than that near the other electrode. The pronounced difference between the photoconductivity spectra for negative and positive electrode illumination, therefore, can be attributed to the large mobility-lifetime product ($\mu\tau$) for electrons as compared to that for holes. Also, in all the photoconductivity spectra, it is noticed that the peak position under positive electrode illumination occurs at a slightly higher wavelength. The onset of the surface recombination of holes at a higher wavelength than that of electrons may be responsible for this difference. Further, it is observed that the peak photocurrent has a maximum at around 170 K in all the three types of crystals (Fig. 9). This may be due to the thermal ionization of the slow retrapping type electron trapping centres[17,19] at about 0.31 eV, which releases trapped charge carriers and thereby increase the overall photoconductivity. From the peak wavelengths, the values of band gap energy (E_g) at different temperatures were estimated using the

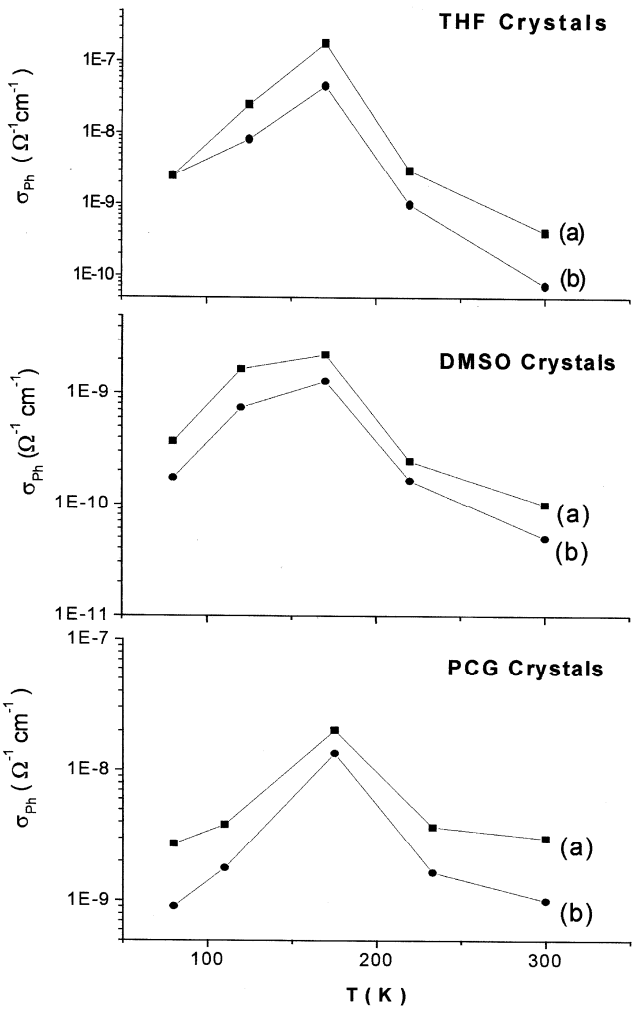

Fig. 9 — Temperature dependence of the peak photoconductivity for α-HgI_2 crystals of three types: (a) under the negative electrode illumination and (b) under the positive electrode illumination

relationship: E_g (in eV) = $\frac{1.24}{\lambda(\text{in } \mu m)}$. Fig. 10 shows the temperature dependence of the band gap energy for the three types of crystals. Clearly, the temperature dependence is quite linear except at low temperatures. The temperature coefficient of the band gap energy was determined from the linear parts of these curves and was found to be about (-4.1×10^{-4}) eV/K, a value which matched reasonably well with the values recently reported by Burger and Nason[18].

In the slowly varying region of the photoconductivity spectra, for each of the three types of crystals, the light is totally absorbed within a very thin layer (i.e., within a few micrometres) of the sample close to the illuminated surface. This gives

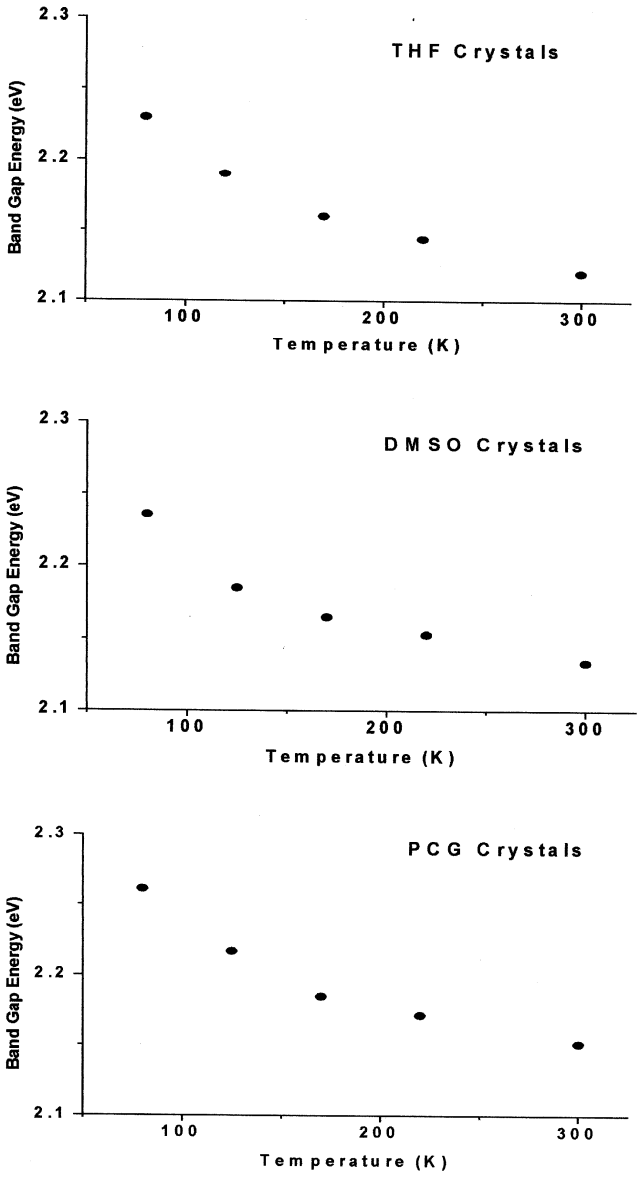

Fig. 10 — Temperature variation of the band gap energy (E_g) for α-HgI_2 crystals of three types

rise to the photoconductivity strongly dominated by the surface and near-surface contributions. Therefore, the photocurrent under negative electrode illumination is mainly due to electrons and that under positive electrode illumination is mainly due to holes. From the photoconductivity spectra, for each of the three types of crystals, it was observed that the wavelength dependence of the photocurrent under the positive electrode illumination is quite weak as compared to that under the negative electrode illumination for the wavelengths below 550 nm. This may probably be due to two different reasons: (i) the surface recombination velocity for electrons may be increasing with photon energy and (ii) the density of the electron recombination centres may be non-uniform in the surface region and has a maximum value at the top of the illuminated surface. Recently, Burshtein *et al.*[9] have also reported the photon energy dependence of the electron surface recombination velocity.

For determining the charge carrier transport properties for each of the three types of α-HgI_2 crystals, the corresponding room temperature photoconductivity spectrum was simulated theoretically. For the theoretical simulation of a photoconductivity spectrum, we have utilized the presently determined absorption coefficients and quantum efficiencies for different wavelengths, μ_e = 100 cm^2/V.s, μ_h = 15 cm^2/V.s, τ_e = 4 μs, τ_h = 0.75 μs, and $S_e = S_h = 10^5$ cm/s. The surface recombination thickness was taken to be about 5 μm. The values of other parameters were set according to the present experimental conditions. For each of the three types of crystals, the quantum efficiency at a wavelength was determined from the photocurrent at that wavelength under the negative electrode illumination in a sample of thickness of about 40 μm. As the quantities αd and d/d_e are both much smaller as compared to unity for the sample of thickness of about 40 μm, for each of the three types of crystals, the corresponding photocurrent density under the negative electrode illumination can be expressed as

$$J^{(-)} = q\,\beta\,\alpha\,I_0\,d \qquad \ldots(14)$$

Thus, the corresponding quantum efficiency can be evaluated from the relationship:

$$\beta = \frac{J^{(-)}}{q\,\alpha\,I_0\,d} \qquad \ldots(15)$$

The variations of the quantum efficiency with wavelength for the three types of α-HgI_2 crystals, so obtained, are shown in Fig. 11. The mobility-lifetime products of the two charge carriers ($\mu_e\tau_e$, $\mu_h\tau_h$) were first optimized such that the simulated spectrum matched reasonably well with the experimental spectrum in the weak absorption region (590 nm < λ < 700 nm). This is quite reasonable because, in this region, the surface contribution to the total photocurrent is negligibly small. Using these optimized values of the mobility-lifetime products,

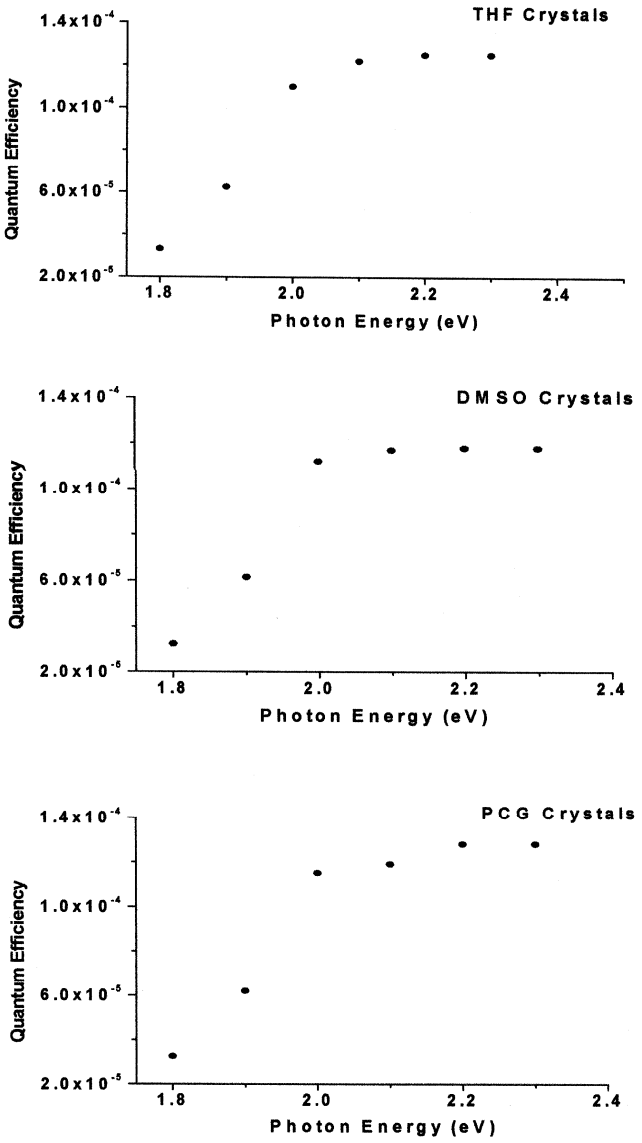

Fig. 11 — Wavelength dependence of the quantum efficiency (β) for α-HgI_2 crystals of three types

once again, the total photoconductivity spectrum was generated. It was seen that the simulated spectrum deviated from the experimental spectrum only in the strong absorption region (450 nm < λ < 550 nm). Subsequently, the values of the surface recombination velocities (S_e, S_h) were optimized in order to match the simulated spectrum with the experimental spectrum in the strong absorption region where the bulk contribution is negligibly small compared to the surface contribution. Table 2 lists the optimized values of all the transport parameters for the α-HgI_2 crystals of three types. Except the values of S_e, the values of all other parameters for the samples of three types match fairly well with the values reported in the literature for nuclear radiation detector grade crystals[27]. The values of the surface recombination velocity for electrons (S_e) for the three types of samples are almost an order of magnitude higher than the value reported by Levi *et al.*[12,27]. Obviously the surface conditions improve on etching, however, the same are not optimal as regards to the electron surface recombination.

Table 2 — Optimized carrier transport properties for the α-HgI_2 crystals of three types

Property	THF crystals	DMSO crystals	PCG crystals
$\mu_e\tau_e$ (cm^2/V)	5.65×10^{-5}	6.65×10^{-5}	3.15×10^{-4}
$\mu_h\tau_h$ (cm^2/V)	1.81×10^{-6}	2.45×10^{-6}	6.80×10^{-6}
S_e (cm/s)	3.21×10^{5}	3.82×10^{5}	2.11×10^{5}
S_h (cm/s)	4.52×10^{5}	5.01×10^{4}	3.61×10^{4}

For the electric field strength of about 2×10^3 V/cm, the electron drift lengths for the three types of crystals were 1150 μm, 1350 μm and 6500 μm, respectively, while the hole drift lengths were 50 μm, 50 μm and 150 μm, respectively. As the typical thickness of α-HgI_2 photodetector for its use in any scintillation spectrometer is about 300 μm, all the three types of crystals under negative electrode illumination possess high potential for their use as photodetectors in conjunction with most of the scintillating materials. Further work is in progress to simulate the photoconductivity spectra recorded at low temperatures in order to determine the temperature dependence of different transport properties and to study the performance of different α-HgI_2 photodetector based scintillation spectrometers.

5 Conclusions

The photoconductivity spectra for the α-HgI_2 crystals of three types, at all temperatures, show a sharp rise on lowering the wavelength from 700 nm to 600 nm (the weak absorption region), pass through a maximum within the wavelength range 600-550 nm and finally go to a slowly varying region below 550 nm (the strong absorption region). Analyses show that the photoconductivity in the weak absorption region is

mainly governed by the bulk processes while that in the strong absorption region is totally controlled by the generation and recombination of charge carriers on and near the surface. The peak photocurrent goes through a maximum at about 170 K. The occurrence of this maximum in the peak photocurrent may be associated with the slow retrapping type electron traps at 0.31 eV, which get thermally ionized around this temperature and contribute to the overall photoconductivity. From the temperature dependence of the peak wavelength, the temperature coefficient of the band gap was found to be about $(-\ 4.1\times10^{-4})$ eV/K. By simulation of the room temperature photoresponse, the optimized values of the mobility-lifetime products and surface recombination velocities for electrons and holes for the α-HgI_2 crystals of the three types have been determined. The estimates of the drift lengths for the two charge carriers suggest that, under the negative electrode illumination, all the three types of α-HgI_2 crystals can be used as photodetectors in conjunction with most of the scintillating materials. Further work is in progress to simulate the photoconductivity spectra recorded at low temperatures in order to determine the temperature dependence of different transport properties and to study the performance of different α-HgI_2 photodetector based scintillation spectrometers.

References

1 Armantrout G A, Swierkowski S P, Sheroman J W & Yee J H, *IEEE Trans Nucl Sci*, 24 (1977) 121.

2 Lamonds H A, *Nucl Instrum Meth*, 213 (1983) 5.

3 Iwanczyk J S, Barton J B, Dabrowski A J, Kusmiss J H, Szymczyk W M, G C Huth, Markakis J, Schnepple W F & Lynn R, *Nucl Instrum Meth*, 213 (1983) 123.

4 Iwanczyk J S, Barton J B, Dabrowski A J, Kusmiss J H & Szymczyk W M, *IEEE Trans Nucl Sci*, 30 (1983) 363.

5 Iwanczyk J S, Dabrowski A J, Markakis J, Ortale C & Schnepple W F, *IEEE Trans Nucl Sci*, 31 (1984) 336.

6 Markakis J, Ortale C, Schnepple W F, Iwanczyk J S & Dabrowski A J, *IEEE Trans Nucl Sci*, 32 (1985) 559.

7 Bube R H, *Phys Rev*, 106 (1957) 703.

8 Momammed-Brahim T, Friant A & Mellet J, *Phys Status Solidi (a)*, 79 **(**1983) 71.

9 Burshtein Z, Akujieze J K & Silberman E, *J Appl Phys*, 60 (1986) 3182.

10 Bornstein J & Bube R H, *J Appl Phys*, 61 (1987) 2676.

11 Many A, *J Phys Chem Solids*, 26 (1965) 575.

12 Levi A, Burger A, Schieber M M, Van den Berg L, Yelton W B & Alkire R W, *Nucl Instrum Meth*, 213 (1983) 31.

13 De Vore H B, *Phys Rev*, 102 (1956) 86.

14 Bohac P, *J Crystal Growth*, 61 (1983) 163.

15 Nicolau Y F, *J Crystal Growth*, 48 (1980) 61.

16 Faile S P, Dabrowski A J, Huth G C & Iwanczyk J S, *J Crystal Growth*, 50 (1980) 752.

17 Pal T, Sharma S L & Acharya H N, *J Phys D*, 28 (1995) 1439.

18 Burger A & Nason D, *J Appl Phys*, 71 (1992) 2717.

19 Schlesigner T E, Bao X J, James R B, Cheng A Y, Ortale C & Van den Berg L, *Nucl Instrum Meth in Phys Res*, A 322 (1992) 414.

20 De Blasi C, Galassini S, Manfredotti C, Micocci G, Ruggiero L & Tepore A, *Nucl Instrum Meth*, 150 (1978) 103.

21 Tadjine A, Gosselin D, Koebel J M & Siffert P, *Nucl Instrum Meth*, 213 (1983) 77.

22 Suryanarayana P, Acharya H N & Nicolau Y F, *Semicond Sci Technol*, 7 (1992) 297.

23 Hyder S B, *J Appl Phys*, 48 (1977) 313.

24 Merz J L, Wu Z L, Van den Berg L & Schnepple W F, *Nucl Instrum Meth*, 213 (1983) 51.

25 James R B, Bao X J, Schlesinger T E, Cheng A Y, Ortale C & Van den Berg L, *Nucl Instrum Meth Phys Res*, A 322 (1992) 435.

26 Lopez-Cruz E, *J Appl Phys*, 65 (1989) 874.

27 Levi A, Schieber M M & Burshtein Z, *J Appl Phys*, 54 (1983) 2472.